Loading on Long Span Bridges in Heavily Trafficked Areas

Michael Quilligan[12], Eugene J. OBrien[2]
[1]School of Engineering, University of Limerick, Limerick, Ireland
[2]School of Civil Engineering, University College Dublin, Ireland
email: michael.quilligan@ul.ie, eugene.obrien@ucd.ie

ABSTRACT: The critical traffic loading condition for long-span bridges is congestion when vehicles may be closely spaced together. Data on very high traffic flows is limited however, as induction loops which are typically used to collect traffic data, are ineffective when traffic flow breaks down. A number of long span bridges are located in areas of high traffic with periods of recurring congestion occurring daily. While the inter-vehicle gap distances are greater than those occurring during non-recurring full stop accident type events, the high frequency of the recurring congestion events can increase the probability of a critical load case occurring. A location on the N7/M7 national primary route in Ireland is identified where regular congestion occurred due to a lane drop. Traffic monitoring using an Unmanned Aerial Vehicle (UAV) is carried out, generating a significant amount of high quality footage of congested traffic from a bird's eye view. A method of processing the data is developed to transform the trajectory data into a traffic stream that can be used to simulate load effects on long span structures. The process is applied to 2 notional long span structures. Insights into the load patterns that give rise to critical loading events are identified for both structures.

KEY WORDS: Unmanned Aerial Vehicle; UAV; Traffic; Congestion; Bridge; Loading; Long-span.

1 INTRODUCTION

Unlike short to medium span bridges where individual heavy concentrations in free flowing traffic produce the maximum load effect, the critical loading events for long span structures are caused by congested traffic [1-4]. During congestion events, the gaps between vehicles reduce and the cumulative effect of closely spaced vehicles produces the critical load events. The accurate evaluation of traffic loading patterns on long span bridges is however problematic. Traffic data, traditionally collected with inductive loop detectors, does not provide accurate information about congested traffic as the loops are generally ineffective in stop-and-go conditions [5]. Existing load models account for the variability of truck weights using Weigh-in-Motion (WIM) data; however data on the car/truck mix and inter-vehicle gaps during congested conditions is limited [4, 6-8]. Excessive conservatism in such assumptions can lead to expensive and unnecessary interventions in existing bridges.

Recent studies have used micro-simulation as a means to better represent traffic modelling on long-span bridges. Cellular automation, where the bridge is divided into cells and lane changing is considered but not the variability of vehicle lengths and gaps [9]. Other approaches combined car following and lane changing models [8, 10-14], and have shown that the critical condition for long span loading is not always the widely-used full-stop condition, but can be slow moving traffic [8, 15]. This occurs because full-stop queues consider only one realisation of vehicles on the bridge, which reduces the probability of having an extreme loading scenario. A drawback of micro-simulation models however is that there is limited data available to calibrate the vehicle behaviour models [16, 17].

Image processing and computer vision approaches are being used increasingly for traffic data surveys [18-20]. The methods are suitable for detecting and classifying vehicles in different traffic conditions, allowing the evaluation of traffic densities and vehicle velocities [21, 22].

Previous bridge loading studies have made use of video data of traffic, albeit in limited quantities [4, 23]. Data on the lane changing behaviour of cars and Heavy Goods Vehicles (HGV), both in free-flowing and congested traffic, was analysed using video data recorded at several sites in the United Kingdom [24]. More extensive recent studies have used 5 months of video images, collected from a fixed camera attached to the tower of a suspension bridge, to determine maximum load effects using statistical correlations between vehicle lengths and their weights [25, 26]. Data on heavily congested events was limited however.

The range of applications for Unmanned Aerial Vehicles (UAVs) has increased significantly in recent years [27]. UAVs offer a number of significant advantages for traffic monitoring applications in that: they are portable and easily transferable to areas of interest; they can collect data from an extended road section from a bird's eye view without affecting drivers' behaviour; and they are cost effective when compared to fixed or manned solutions [28-31]. Recent studies have shown that low cost UAV can provide reliable traffic data parameters with appropriate stabilising and geo-referencing of the video data [30, 32].

This study investigates the novel use of a UAV to monitor congested traffic conditions and develop insights into critical loading patterns on long span bridges. Video footage is collected at a location on a national primary route in Ireland with regular recurring congestion caused by a lane drop. The video data is analysed using an automated image processing algorithm and transformed to real world coordinates using a geo-referencing process. A method of processing the data is developed to transform the trajectory data into a traffic stream

that can be used to simulate load effects on long span structures. The process is applied to two notional long span structures.

2 TRAFFIC MONITORING

2.1 Site Description

The N7/M7 is a national primary route connecting Dublin and the south of Ireland, serving the cities of Limerick (M7), Cork (M8) and Waterford (M9). It forms part of the E20 European route. The N7 commences at Junction 9 of the M50 to the southwest of Dublin. It is a three lane carriageway in each direction for 20 km until Junction 9 Naas North, with an Annual Average Daily Traffic (AADT) flow of approximately 105,000 vehicles. From Junction 9 onwards the route becomes full motorway standard. Prior to 2019 the number of lanes reduced to 2 at this location, causing a significant recurring congestion to occur during evening rush hour periods.

A contour plot of the mean traffic velocities on the N7/M7 for vehicles travelling towards the southwest (away from Dublin) on a sample evening is illustrated in Figure 1. The plot is constructed using data from 7 traffic counter sites operated by Transport Infrastructure Ireland, with linear interpolation of velocities in between. While some congestion is evident at the start of the route as vehicles join from the M50, it is clear that the lane drop at Junction 9 results in significant congestion from approximately 16.30-18.00 (Figure 2).

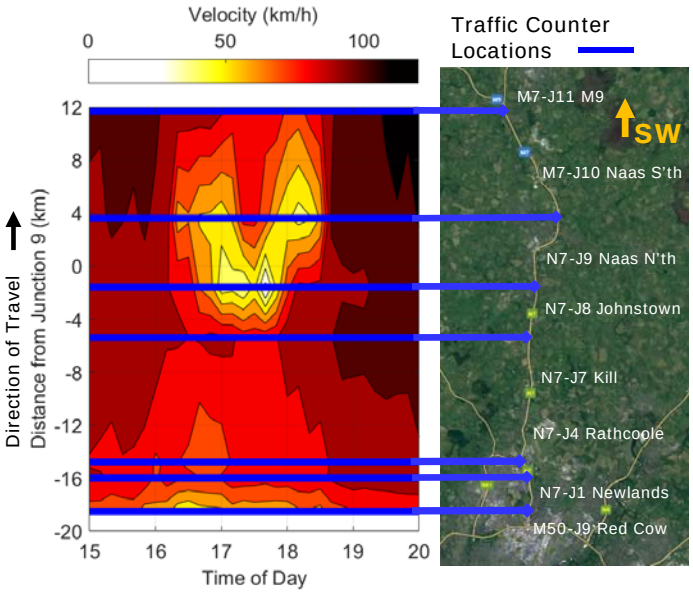

Figure 1. Space-time-velocity contour plot for N7/M7 (15.05.2017)

A survey of the area around Junction 9 was undertaken to identify potential sites to operate a UAV and monitor the recurring congestion. An area of agricultural ground was identified adjacent to the lane drop location, close to the village of Johnstown on the outskirts of Naas (Figure 3). The site allowed for the flying of the UAV within the operational limits of the Irish Aviation Authority (IAA) without requiring specific operating permission [33]. Notwithstanding this, a detailed operations manual was prepared with risk assessments and operating procedures developed to ensure safe operation at all times. The landowner and leaseholder were also notified.

Figure 2. View of lane drop from UAV: Lane 1 (R445) exits to Naas (centre background), Lanes 2&3 (N7/M7) continue to southwest

Construction work to widen the M7 from Junction 9 to Junction 11 to 3 lanes started in January 2018, with the extra lane coming into operation in August 2019. Traffic monitoring at the Johnstown site for this project took place between August and October 2018. Carriage realignment to facilitate the downstream widening works provided lane widths of approximately 3.25, 3.50 and 3.25m at the UAV site location.

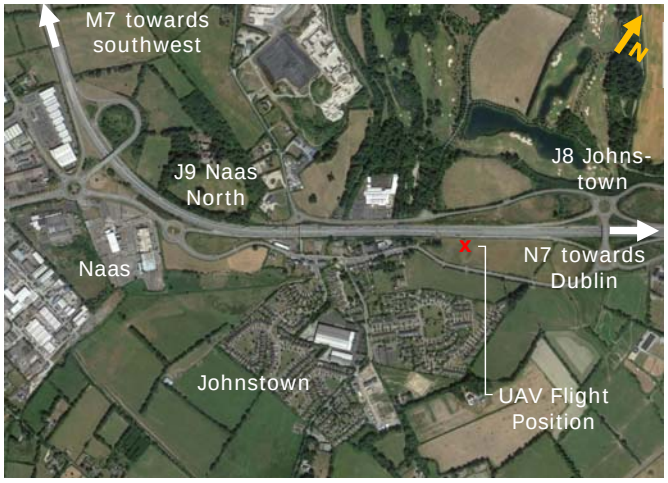

Figure 3. Aerial view of UAV flight position between Junctions 8 and 9, Johnstown, Naas, Ireland [34]

2.2 Data Collection

Traffic footage was collected using a DJI Phantom 4 Advanced quadrotor which has a 20-megapixel camera (Figure 4). Videos were recorded in 4K (4096×2160) resolution at 25 frames-per-second. Allowing for take-off, landing and a safe reserve of battery power, an average of 20 minutes traffic footage was collected for each flight. The turnaround time to fly back to the landing site, change battery and return to the hovering location was approximately 5 minutes. A maximum recording time of 100 minutes was possible using 4 batteries, one of which could also be re-charged on site using a car charger. The car charging time for a single battery was 70 minutes. Video footage was

collected on micro SD memory cards, which were changed between flights to allow regular download and backup of the data. A limitation of the UAV equipment is that data collection is restricted to periods of no rain and wind speeds less than 35 km/h.

Figure 4. DJI Phantom 4 Advanced used for the traffic monitoring

The coordinates of the hovering location were pre-programmed to ensure consistent positioning for each flight. The UAV was hovered at a height of 120 m and a distance of 30 m from the edge of the carriageway (Figure 5). This maximised the length of road captured, while remaining within the operational limits specifying by the IAA [33]. At this height the road length captured was approximately 165 m, with a ground sampling distance of approximately 4.3 cm. The camera was pointed directly downwards during filming to maximise the accuracy when locating ground targets [35].

Figure 5. View from UAV at 120 m hovering height

Data was collected on 20 different days. A total of 71 flights were flown, resulting in 862 GB of video data and 22 hours of congested traffic footage.

3 IMAGE PROCESSING

The video footage was analysed using DataFromSky (DFS), a cloud-based platform that specialises in automated traffic analysis. The system processes traffic data in two stages: 1) detection, localisation and tracking of objects of interest; 2) mapping between the video frames and a real-world coordinate system, a process termed ‘georegistration’.

A deep learning convolution neural network algorithm is used by DFS to detect the objects of interest (vehicles). To improve performance and robustness, potential vehicles are pre-filtered by the expected area of road surface and the results of a moving object detection algorithm. Vehicles are then matched and tracked through the video sequence. Using vehicle kinematic models, the vehicle trajectories are filtered to reduce localisation noise to ensure that small tracking errors will not result in sudden changes in positioning [35].

For the geo-referencing process, a minimum of four points of known position are identified by the operator and then used to estimate a transformation to map the data from an image space to a coordinate space, assuming that the road surface is planar. A distortion correction is also applied to the video sequence [36].

The DFS platform has been used in a number of recent studies and has been shown to provide accurate data, particularly when the geo-referencing process in undertaken correctly [28, 32].

The following tasks were undertaken to process the N7 data using DFS:

- Join videos to create single video file per flight. (The UAV software automatically segments videos to limit file sizes to less than 4 GB. A single flight averaged 16 GB);
- Upload video to the DFS website and submit for analysis;
- Download processed tracking file and view using DFS Viewer software;
- Geo-reference tracking file using DFS Viewer;
- Export raw telemetry data for further analysis.

A typical view of the geo-referenced data in the DFS Viewer is illustrated in Figure 6. The software offers a number of post processing functions; however only the raw vehicle trajectory data was used in this work.

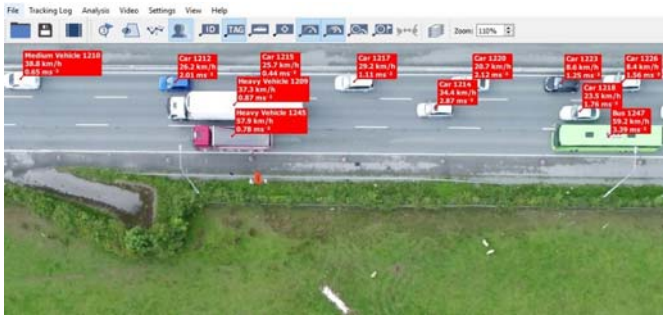

Figure 6. DFS Viewer interface with vehicle identification, velocities and accelerations displayed

4 DATA PROCESSING

4.1 Trajectory Data

The vehicle trajectory data for Lane 2 (slow) of a sample flight is illustrated in Figure 7. This space-time plot is feature rich, detailing the location data of all vehicles in the captured road length during the 20 minute flight. Each (blue) line represents the trajectory of a vehicle, with vehicles travelling from lower left to upper right. A horizontal trajectory indicates a vehicle at rest, with no change in space (Y-axis) for increasing time (X-

axis). The slope of the trajectory increases with increasing vehicle velocity.

A vertical line through the data details the position of each vehicle at that point in time. The solid (red) line shown at approximately 5 minutes illustrates a period of high density with 17 vehicles at rest, equivalent to 103 veh/km.

A horizontal line through the data details the time that each vehicle passes a point in space. The dashed (red) line shown at 80 m illustrates the three primary stop-go-waves that occurred at approximately 5, 12 and 18 minutes.

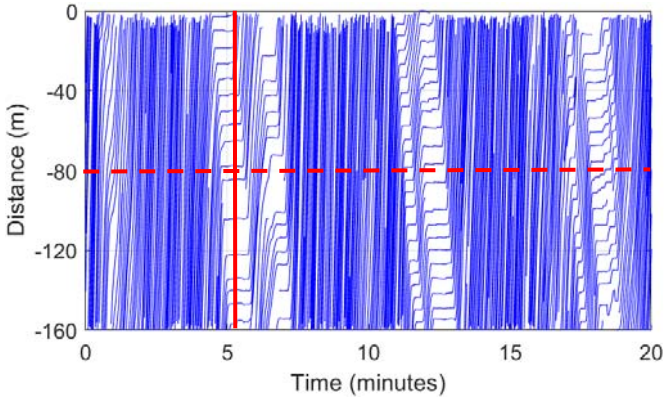

Figure 7. Vehicle space-time trajectories for Lane 2 of sample video (23.10.2018-V1)

4.2 *Density vs Time/Space*

The density of the captured roadway length is determined from the trajectory data at a frame rate of 1 second and scaled to 1 km. The resultant density-time plots are illustrated in Figure 8a for Lane 2 (slow) and Lane 3 (fast) of the N7. The features of the stop-go-waves evident in the trajectory data are clearly present. It is notable that the traffic patterns are not identical in both lanes, with a greater frequency of congested traffic in Lane 3.

To facilitate the determination of bridge load effects it is important to transform the data, recorded in a time reference, to a space reference. The proposed transform is given in Equation 1:

$$dx_i = \bar{v}_i \times T \quad (1)$$

where dx_i is the space transform for frame i, $\bar{v}_i$ is the mean velocity for all vehicles in frame i (m/s) and T is the sampling period (s). The mean velocity can be calculated directly from the DFS data. Figure 8b illustrates the density-time and mean velocity-time plots for the sample video. It is clear that mean velocity is inversely proportional to density.

The transformed data is plotted in Figure 8c. The effect of the transform is to scale the X-axis, i.e. the axis is stretched when the mean velocity is high (flowing traffic) and squashed when the mean velocity is low (congested traffic). The resultant data is equivalent to a traffic stream approximately 8.5 km in length.

4.3 *Equivalent Load vs Space*

The next stage in the data processing is to account for the weight of vehicles in the traffic stream. Inferring vehicle weight from their length has been shown to be suitable for long span bridge load effects [26]. While a WIM site is located 5.4 km upstream of the test location on the N7, constant weights of 20 kN for cars and 300 kN for Heavy Goods Vehicles (HGVs) are used for this study. These values allow an Equivalent Uniformly Distributed Load (EUDL) to be determined for each frame. Figure 8d illustrates the resultant EUDL-time plots for each lane.

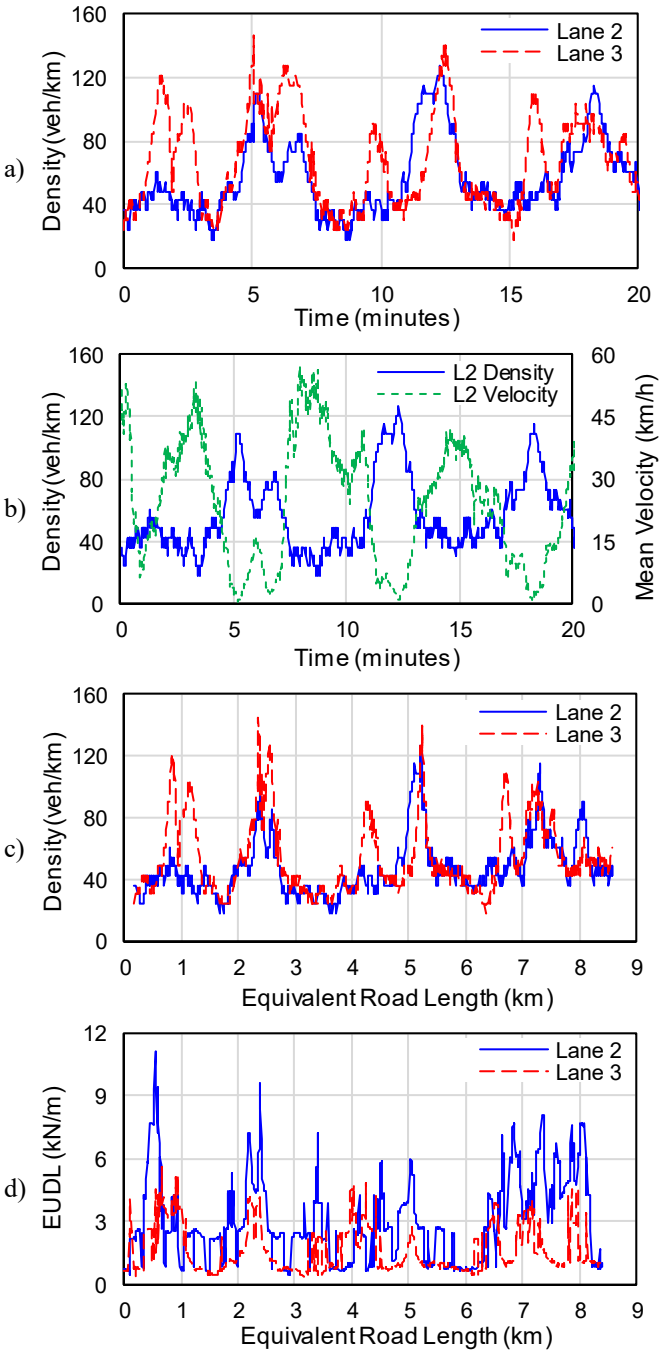

Figure 8. a) Density vs time; b) Density & velocity vs time; c) Density vs space; d) Equivalent Uniformly Distributed Load (EUDL) vs space for sample video (23-10-2018-V1)

It is evident from the comparison of Figure 8c and d that high density does not directly correlate to high loading. While Lane 3 has a higher frequency of high-density events, the EUDL is generally lower due to the small percentage of HGVs present in this lane. In Lane 2 a number of high individual EUDL peaks are present from 0-5 km, with a series of closely spaced peaks present from 6.5-8 km.

It is to be noted that the general magnitude of the EUDLs are low, due in the main to the low percentage of HGVs present – approximately 8% for this traffic video.

One reason that areas of high EUDL do not correlate to high density relates to the method of density calculation. Figure 9 illustrates a screenshot taken from the traffic stream at the equivalent road length of 0.5 km (Figure 8d). The Lane 2 density is a low-moderate 48 veh/km based on 8 vehicles in the 165 m length. However the spatial density, a measure of the percentage of road length occupied, is a moderate-high 60% due to the number of HGVs present.

Figure 9. Screenshot from traffic stream

The adoption of a spatial density measure is therefore preferable as it can provide greater insights into critical traffic patterns. However, this is not currently possible with DFS as vehicle lengths are not outputted.

5 BRIDGE LOAD EFFECTS

To determine the effect of the traffic stream on long span bridges, two structures with loaded lengths of 500 and 1500 m are studied. A total load influence line is adopted which is representative of long span load effects. The responses of the structures are simulated by passing the vehicle stream developed from Figure 8d over each influence line.

Figure 10 illustrates the normalised load effect plots for each loaded length under Lane 2 (slow) loading. These graphs provide an insight into what parts of the traffic stream give rise to critical load effects.

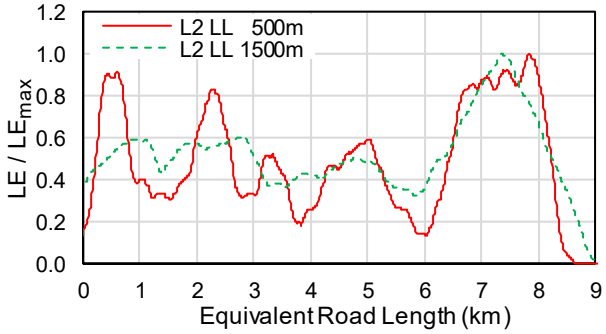

Figure 10. Normalised load effect plots for 500 and 1500 m loaded lengths

For the longer 1500 m loaded length, the critical load case is caused by the series of closely spaced EUDL peaks from 6.5-8 km. The high individual EUDL peaks have a much smaller effect, with normalised values less than 0.6. For the 500 m loaded length, while the critical load case remains the series of closely spaced peaks, the individual peaks have a greater effect with normalised values of 0.83 and 0.90.

6 CONCLUSIONS

This paper investigates the novel use of a UAV to monitor congested traffic conditions and develops insights into critical loading patterns on long span bridges.

A location on the N7/M7 national primary route in Ireland was identified where regular recurring congestion occurred due to a lane drop. Traffic monitoring using a UAV was successfully carried out, generating a significant amount of high quality footage of congested traffic from a bird's eye view.

A method of processing the data was developed to transform the trajectory data into a traffic stream that could be used to simulate load effects on long span structures. The process was applied to 2 notional long span structures. Insights into the load patterns that give rise to critical loading events were identified for both structures.

ACKNOWLEDGEMENTS

The authors would like to acknowledge the work of Stephen Lynch in helping with the data collection phase of the work. The authors would also like to thank RCE Systems s.r.o. for access to the DataFromSky platform, and to Transport Infrastructure Ireland for access to the traffic counter data.

REFERENCES

[1] Ivy, R., Lin, T., Mitchell, S., Raab, N., Richey, V., and Scheffey, C., *Live loading for long-span highway bridges.* American Society of Civil Engineers Transactions, 1954.

[2] Buckland, P.G., McBryde, J.P., Zidek, J.V., and Navin, F.P.D., *Proposed Vehicle Loading of Long-Span Bridges.* Journal of the Structural Division, 1980. **106**(4): p. 915-932.

[3] Flint & Neill Partnership, *Interim design standard: long span bridge loading*. 1986: Crowthorne.

[4] Lutomirska, M. and Nowak, A.S. *Site-specific live load and extreme live load models for long span bridges*. in *Safety, Reliability, Risk and Life-Cycle Performance of Structures and Infrastructures - Proceedings of the 11th International Conference on Structural Safety and Reliability, ICOSSAR 2013*. 2013.

[5] Klein, L.A., Mills, M.K., and Gibson, D.R., *Traffic detector handbook: Volume I*. 2006, Turner-Fairbank Highway Research Center.

[6] Bruls, A., Calgaro, J.A., Mathieu, H., and Prat, M., *ENV1991 – Part 3: The main models of traffic loads on bridges; background studies*, in *IABSE Colloquim*. 1996: Delft, The Netherlands. p. 215-228.

[7] Hwang, E.-S. and Kim, D.-Y., *Live Load Model for Long Span Steel Cable Bridges Considering Traffic Congestion Scenarios.* International Journal of Steel Structures, 2019. **19**(6): p. 1996-2009.

[8] Caprani, C.C., OBrien, E.J., and Lipari, A., *Long-span bridge traffic loading based on multi-lane traffic micro-simulation.* Engineering Structures, 2016. **115**: p. 207-219.

[9] Chen, S.R. and Wu, J., *Modeling stochastic live load for long-span bridge based on microscopic traffic flow simulation.* Computers & Structures, 2011. **89**(9-10): p. 813-824.

[10] Caprani, C. *Using microsimulation to estimate highway bridge traffic load*. in *Proc. 5th Intl. Conf. on Bridge Maintenance, Safety and Management*. 2010.

[11] Enright, B., Carey, C., and Caprani, C.C., *Microsimulation evaluation of Eurocode load model for American long-span bridges.* Journal of Bridge Engineering, 2013. **18**(12): p. 1252-1260.

[12] Lipari, A., Caprani, C.C., and OBrien, E.J., *A methodology for calculating congested traffic characteristic loading on long-span bridges using site-specific data.* Computers & Structures, 2017. **190**: p. 1-12.

[13] Carey, C., Caprani, C.C., and Enright, B., *A pseudo-microsimulation approach for modelling congested traffic loading on long-span bridges.* Structure and Infrastructure Engineering Maintenance, Management, Life-Cycle Design and Performance, 2018. **14**(2): p. 163-176.

[14] Zhou, J., Ruan, X., Shi, X., and Caprani, C.C., *An efficient approach for traffic load modelling of long span bridges.* Structure and Infrastructure Engineering, 2019: p. 1-13.

[15] OBrien, E.J., Lipari, A., and Caprani, C.C., *Micro-simulation of single-lane traffic to identify critical loading conditions for long-span bridges.* Engineering Structures, 2015. **94**: p. 137-148.

[16] Lipari, A., *Micro-simulation modelling of traffic loading on long-span bridges*, in *School of Civil, Structural and Environmental Engineering*. 2013, University College Dublin.

[17] OBrien, E.J., Hayrapetova, A., and Walsh, C., *The use of micro-simulation for congested traffic load modeling of medium- and long-span bridges.* Structure and Infrastructure Engineering, 2012. **8**(3): p. 269-276.

[18] Klein, L., Mills, M., and Gibson, D., *Traffic detector handbook (Vol 2)*. 2006, Federal Higway Administration: MacLean, Virginia.

[19] Osuto, D.A., *Vision based road traffic density estimation and vehicle classification for stationary traffic scenes.* JOURNAL OF SUSTAINABLE RESEARCH IN ENGINEERING, 2016. **2**(3): p. 100-110.

[20] Minge, E., Kotzenmacher, J., and Peterson, S., *Evaluation of non-intrusive technologies for traffic detection*. 2010, Minnesota Department of Transportation, Research Services Section.

[21] Coifman, B., Beymer, D., McLauchlan, P., and Malik, J., *A real-time computer vision system for vehicle tracking and traffic surveillance.* Transportation Research Part C: Emerging Technologies, 1998. **6**(4): p. 271-288.

[22] Reinartz, P., Lachaise, M., Schmeer, E., Krauss, T., and Runge, H., *Traffic monitoring with serial images from airborne cameras.* ISPRS Journal of Photogrammetry and Remote Sensing, 2006. **61**(3-4): p. 149-158.

[23] Buckland, P.G., McBryde, J.P., Navin, F.P.D., and Zidek, J.V., *Traffic loading of long span bridges.* Transportation Research Record No. 665, Bridge Engineering, 1978. **2**.

[24] Ricketts, N.J. and Page, J., *Traffic data for highway bridge loading.* Transport Research Laboratory. Report 251., 1997.

[25] Micu, E.A., Malekjafarian, A., OBrien, E.J., Quilligan, M., McKinstray, R., Angus, E., Lydon, M., and Catbas, F.N., *Evaluation of the extreme traffic load effects on the Forth Road Bridge using image analysis of traffic data.* Advances in Engineering Software, 2019. **137**.

[26] Micu, E.A., OBrien, E.J., Malekjafarian, A., and Quilligan, M., *Estimation of Extreme Load Effects on Long-Span Bridges Using Traffic Image Data.* The Baltic Journal of Road and Bridge Engineering, 2018. **13**(4): p. 429-446.

[27] Pajares, G., *Overview and Current Status of Remote Sensing Applications Based on Unmanned Aerial Vehicles (UAVs).* Photogrammetric Engineering & Remote Sensing, 2015. **81**(4): p. 281-330.

[28] Barmpounakis, E. and Geroliminis, N., *On the new era of urban traffic monitoring with massive drone data: The pNEUMA large-scale field experiment.* Transportation Research Part C: Emerging Technologies, 2020. **111**: p. 50-71.

[29] Barmpounakis, E.N., Vlahogianni, E.I., and Golias, J.C., *Unmanned Aerial Aircraft Systems for transportation engineering: Current practice and future challenges.* International Journal of Transportation Science and Technology, 2016. **5**(3): p. 111-122.

[30] Wang, L., Chen, F., and Yin, H., *Detecting and tracking vehicles in traffic by unmanned aerial vehicles.* Automation in Construction, 2016. **72**: p. 294-308.

[31] Kanistras, K., Martins, G., Rutherford, M.J., and Valavanis, K.P., *A survey of unmanned aerial vehicles (UAVs) for traffic monitoring*, in *2013 International Conference on Unmanned Aircraft Systems (ICUAS)*. 2013. p. 221-234.

[32] Barmpounakis, E.N., Vlahogianni, E.I., Golias, J.C., and Babinec, A., *How accurate are small drones for measuring microscopic traffic parameters?* Transportation Letters, 2019. **11**(6): p. 332-340.

[33] Small Unmanned Aircraft (Drones) and Rockets Order, SI 563/2015, 2015.

[34] Google Earth. *Johnstown, Co. Kildare, Ireland; 53o14'36"N 6o36'24"W.* 2020 29.04.2020]; Version 9.3.109.1:[http://www.google.com/earth/index.html].

[35] Adamec, V., Herman, D., Schullerova, B., and Urbanek, M., *Modelling of Traffic Load by the DataFromSky System in the Smart City Concept*, in *Smart Governance for Cities: Perspectives and Experiences*, N.V.M. Lopes, Editor. 2020, Springer Nature: Switzerland. p. 135-152.

[36] Adamec, V., Schullerová, B., Herman, D., and Vémola, A. *Possibilities of the traffic emission monitoring in context of the smart cities concept.* in *7th International Scientific Conference of the Faculty of Transportation Engineering*. 2018. Pardubice, Czech Republic.